Dispersion Engineered High-Quality Ge–Sb–S Reflowed Wedge Resonator

Bo Xu, Bright Lu, Michael Topper, Mo Zohrabi, Juliet T. Gopinath, and Wounjhang Park

***Abstract*—Dispersion engineering in chalcogenide integrated photonics is crucial for nonlinear optical applications. We have developed a thermal-reflow-assisted fabrication method that creates $Ge_{23}Sb_7S_{70}$ reflowed wedge resonators with supreme surface roughness and quality factors exceeding 10^6. Our simulations show the ability to engineer the dispersion of their whispering-gallery modes to overcome large material dispersion in near-infrared wavelength and achieve anomalous dispersion. We have successfully fabricated the designed tightly confined reflow bump geometry and experimentally demonstrate an engineered flat anomalous dispersion of the supported TM_{00} optical mode.**

***Index Terms*—Chalcogenide integrated photonics, dispersion engineering, nonlinear optics, thermal reflow fabrication, whispering-gallery mode resonators.**

I. Introduction

THERE is a great need for compact, broadband, high efficiency infrared light sources for applications ranging from telecommunications and spectroscopy to quantum and biomedical technologies [1], [2], [3], [4], [5]. Integrated nonlinear photonics based on chalcogenide glass microresonators offers a potential solution to these needs. Chalcogenide glasses are known for their high nonlinearities, long wavelength transparency, and excellent figure of merit (ratio of nonlinearity to two-photon absorption) [6], [7], [8], [9]. Recent advances in the integrated photonic devices based on $Ge_{23}Sb_7S_{70}$ and $Ge_{28}Sb_{12}Se_{60}$ glasses hold high promises for applications such as Kerr frequency comb generation in the near- and mid-infrared region [10], [11]. Additionally, chalcogenides can be directly deposited onto other optical materials such as III-V semiconductors, lithium niobate, silicon nitride, and other chalcogenides, enabling heterogeneously integrated devices that harness optical properties of multiple materials [12], [13], [14].

Whispering gallery mode (WGM) microresonators have been a popular platform for numerous fundamental investigations due to their micro-scale confinement of light and abundance of structural parameters for optical engineering [15], [16]. Wedge resonators are especially attractive due to their simple fabrication process, easily engineerable structural parameters: radius, thickness, and wedge angle and potential for full monolithic integration with on-chip waveguide devices [17], [18]. Although silica wedge resonators with varying wedge angles from edge to center have been used to achieve broadband dispersion engineering, they require a complicated fabrication process [19]. Thanks to the low glass transition temperature, $Ge_{23}Sb_7S_{70}$ (GeSbS) glass lends itself to a simple thermal reflow process which can create a continuously varying wedge angles from edge to center in a GeSbS wedge resonator [20], [21]. While dry-etched GeSbS waveguides have shown low-loss of 0.2 dB/cm [22], reflowed wedge resonators offer a better potential for achieving ultra-high Q factors compared to dry-etched ring resonators made of the same material, as the thermal reflow significantly reduces the surface roughness to be the level comparable to microspheres and microtoroids [10], [23], [24].

In our previous research, we demonstrated that reflow could significantly reduce the propagation loss of dry-etched chalcogenide rings by 0.79 dB/cm [10]. We also explored dispersion engineering through simulations in reflowed wedge resonators targeting high-order modes [20]. These results motivate us to further investigate reflowed wedge structures and extend dispersion engineering to fundamental modes in wedge resonators, which offer easier access, clearer spectral identification, and greater potential for broadband nonlinear applications such as four-wave mixing, microcomb generation and on-chip quantum light sources [4], [24], [25]. While other materials have been used for microcomb generation [26], [27], GeSbS devices offer distinct advantages such as low temperature deposition compatible with a wide range of substrates, low glass transition temperature, high nonlinearity and low phonon energies. In particular, GeSbS exhibits broad mid- and long-wave infrared transparency window of 0.6 – 22 μm [7], and reflowed wedge resonator can be a promising platform for miniaturized, infrared sensing and spectroscopy applications [2], [11].

Received 17 March 2025; revised 11 May 2025; accepted 10 June 2025. Date of publication 13 June 2025; date of current version 16 August 2025. This work was supported in part by the Air Force Office of Scientific Research under Grant FA9550-23-1-0265 and Grant FA9550-19-1-0364, in part by the Office of Naval Research under Grant N0001419-1-2251, in part by the National Science Foundation under Grant ECCS 2224065, and in part by Defense Advanced Research Projects Agency under Grant W911NF-15-1-062. *(Corresponding author: Wounjhang Park.)*

Bo Xu and Michael Topper are with the Department of Physics, University of Colorado, Boulder, CO 80309 USA (e-mail: bo.xu@colorado.edu; michael.topper@colorado.edu).

Bright Lu and Mo Zohrabi are with the Department of Electrical, Computer, and Energy Engineering, University of Colorado, Boulder, CO 80309 USA (e-mail: bright.lu@colorado.edu; mo.zohrabi@colorado.edu).

Juliet T. Gopinath is with the Department of Physics, the Department of Electrical, Computer, and Energy Engineering, and the Materials Science and Engineering Program, University of Colorado, Boulder, CO 80309 USA (e-mail: julietg@colorado.edu).

Wounjhang Park is with the Department of Electrical, Computer, and Energy Engineering, and the Materials Science and Engineering Program, University of Colorado, Boulder, CO 80309 USA (e-mail: won.park@colorado.edu).

Color versions of one or more figures in this article are available at https://doi.org/10.1109/JLT.2025.3579685.

Digital Object Identifier 10.1109/JLT.2025.3579685

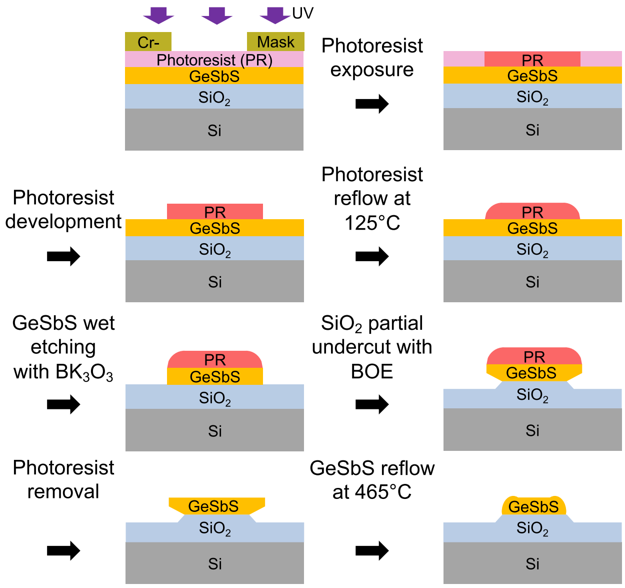

Fig. 1. Fabrication workflow of reflowed wedge resonators. Negative photoresist NR9-1000PY is used as the etch mask. Potassium borate (BK_3O_3) water solution and buffered oxide etch (BOE) are used for $Ge_{23}Sb_7S_{70}$ and SiO_2 wet etching. The reflow of photoresist etch mask at 125 °C greatly reduces the line-edge roughness of the etched $Ge_{23}Sb_7S_{70}$ disk, and the reflow of undercut $Ge_{23}Sb_7S_{70}$ disk at 465 °C significantly improves the surface roughness of the wedge through a rapid melt-quenching.

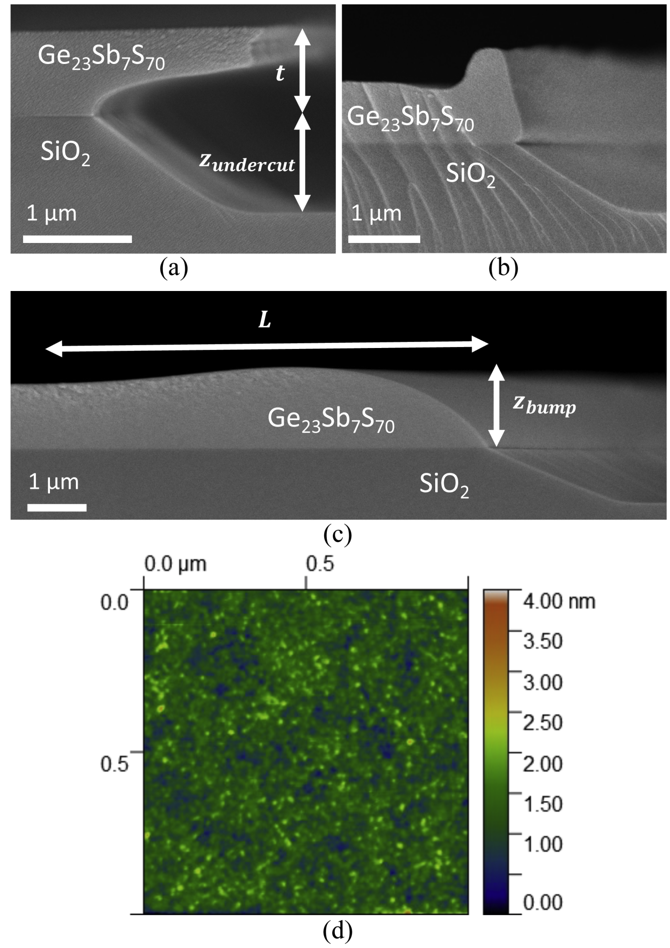

Fig. 2. (a) Scanning electron micrograph of the edge cross-section of a $Ge_{23}Sb_7S_{70}$ microdisk with thickness $t = 0.8$ μm on an undercut SiO_2 pedestal with height $z_{\text{undercut}} = 0.9$ μm. (b) Scanning electron micrograph of the intermediate stage of $Ge_{23}Sb_7S_{70}$ reflow. The $Ge_{23}Sb_7S_{70}$ overhang curls upwards after being melted and reshapes on top of the SiO_2 pedestal. (c) Scanning electron micrograph of the edge cross-section of a $Ge_{23}Sb_7S_{70}$ resonator with reflow bump height $z_{\text{bump}} = 1.42$ μm and reflow bump width $L = 6$ μm. (d) Atomic force micrograph of the reflowed bump top surface shows a surface roughness of 0.3 nm. The micrometer-scale bump curvature background is removed for roughness analysis.

In this paper, we present dispersion engineering with a unique reflowed wedge geometry. We use the geometric dispersion to overcome the material dispersion and achieve a flat and close-to-zero total dispersion in certain optical modes which is a common requirement for many nonlinear operations such as frequency combs, pulse sources, and soliton generation [19], [28], [29], [30]. The in-house fabrication process of GeSbS reflowed wedge resonators will be presented along with the quality factor and dispersion characteristics of the fabricated devices. We report quality factors exceeding 10^6 and demonstrate the ability to engineer the dispersion of WGMs over tens of terahertz bandwidth in the near-infrared region.

II. Dispersion Engineering of Reflowed Wedge Resonators

A. Reflowed Wedge Geometry

We design reflowed wedge resonators as a surface-roughness-improved version of conventional wedge resonators utilizing the low melting temperature of GeSbS glass [20], [21]. A UV-lithography based fabrication process has been developed as shown in Fig. 1. The fabrication starts with the thermal evaporation of the GeSbS thin film on a thermally grown silicon oxide substrate. During the evaporation, the base pressure is 5×10^{-6} Torr and the evaporation rate is $0.2 \sim 1$ nm/s. Then, negative photoresist NR9-1000PY is spin-coated and soft-baked to create a 1-μm-thick resist layer. NR9-1000PY is chosen because its developer (RD6) and stripper (acetone) are compatible with GeSbS glass. A photoresist microdisk is defined by the contact lithography using 365 nm light. It is then reflowed at 125 °C to reduce the line-edge roughness. Next, the GeSbS film is chemically etched by 0.2% (w./w.) potassium borate (BK_3O_3) solution which acts as a buffered potassium hydroxide solution. Then, the 2-μm-thick SiO_2 layer underneath the GeSbS film is undercut by buffered oxide etch (BOE 6:1), which acts as a buffered hydrogen fluoride solution, to create a short silica pedestal. Lastly, the GeSbS microdisk on SiO_2 pedestal is rapidly melted at 465 °C in a tube furnace for $1 \sim 3$ min, and then quenched in air. During this process, the top surface of the wedge becomes extremely smooth and forms a gradually varying slope whose precise shape is controlled by the reflow condition. The reflowed wedge resonator combines the engineerability of microdisks with the excellent surface quality of microtoroids, thanks to the unique properties of GeSbS glass.

The cross-section of the edge area of a GeSbS microdisk before and after the GeSbS reflow step are shown in Fig. 2.

As shown in Fig. 2(a), the BOE not only underetches the silica substrate with a 5 nm/s etch rate, but also mildly attacks the GeSbS at interface with an 8 nm/s horizontal etch rate and 2.5 nm/s vertical etch rate, creating an overhang whose shape depends on the etch time. During the rapid GeSbS melt-quench, the GeSbS overhang first curls upwards and climbs onto the SiO_2 pedestal driven by surface tension, as shown in Fig. 2(b). Then, the GeSbS overhang is melted into a bump shape along the circular edge of the SiO_2 pedestal as shown in Fig. 2(c). According to the thermogravimetric analysis (TGA) of our GeSbS material, there's only negligible vaporization at the reflow temperature. Therefore, as the reflow time increases, gravity and surface tension will shorten and widen the reflow bump, while the radius of the reflowed GeSbS wedge is determined by the underlying SiO_2 pedestal, whose size is well controlled by the BOE etch time. The top surface of the GeSbS reflow bump is characterized by atomic force microscopy (AFM), as shown in Fig. 2(d), and found to have a surface roughness of $\sigma = 0.3$ nm. The bottom surface of the GeSbS reflow bump is the unetched SiO_2 substrate surface, which has a surface roughness measured to be $\sigma = 0.1$ nm. Given the GeSbS thickness t, and the height z_{undercut} and radius R of the silica pedestal, we can control the deformation range during the reflow, L, and determine the expected reflowed wedge profile including the wedge angle at the edge and reflow bump height z_{bump}. To avoid confusion, all these parameters are indicated in Fig. 2(a) and (c). Among these parameters, t is determined by the evaporation rate and time; z_{undercut} is determined by the BOE etch time; R is determined by the lithography and wet etch time; and L is determined by the reflow condition. To simplify the calculation of the expected reflowed wedge profile, we can set the reflowed disk to have the original evaporation thickness in the radius range from 0 to $R-L$. The reflow bump profile curve $z(r)$ in the radius range from $R-L$ to R can be approximated by a 4$^{\text{th}}$ order polynomial: $z(r) = \alpha_0 + \alpha_1 r + \alpha_2 r^2 + \alpha_3 r^3 + \alpha_4 r^4$.

To find the five parameters of the polynomial, we use the three boundary conditions, $z(r = R-L) = t$, $z(r = R) = 0$, $\frac{dz}{dr}|_{r = R-L} = 0$, in addition to the two requirements that the total chalcogenide volume is conserved and the total energy is minimized. That is, we require the deformed volume of the reflowed GeSbS to have the minimum total energy from gravity and surface tension:

$$E_{total} = \int_{R-L}^{R} 2\pi r \left(\rho g \cdot \frac{z(r)^2}{2} + \sigma\sqrt{1+\left(\frac{dz}{dr}\right)^2}\right) dr\,, \quad (1)$$

where ρ is the density of GeSbS known to be 3.15 g/cm^3, g is the gravitational acceleration, $z(r)$ is the reflowed profile function, and σ is the surface tension of melt GeSbS which is determined to be 0.1 N/m from the experimentally measured reflowed wedge profile. Among all available geometry parameters, the deformation range, L, is the hardest to finely tune and radius R is usually set by application requirements for the microresonator's free spectral range (FSR). Thus, t and z_{undercut} are the best tuning parameters to achieve the desired reflow bump height z_{bump}.

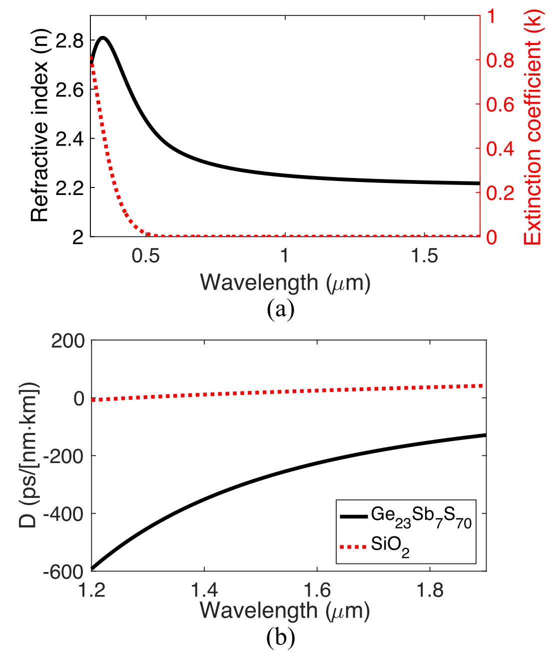

Fig. 3. (a) Refractive index of a 1.1-μm-thick thermally evaporated $Ge_{23}Sb_7S_{70}$ sulfide glass thin film measured by ellipsometry. The refractive index of the film is shown by the black solid line while the extinction coefficient is represented by the red dash line. (b) Material dispersion parameter D spectrum of $Ge_{23}Sb_7S_{70}$ and SiO_2 in near-infrared wavelength range.

B. Dispersion Engineering

For most WGM resonators, material dispersion is the dominant part of their total dispersion due to the lack of subwavelength geometric confinement. To determine the material dispersion of our GeSbS glass, we measured the refractive index of the thermally evaporated thin films by spectroscopic ellipsometry as shown in Fig. 3(a). We fit the averaged index spectrum with Sellmeier equation [31] and obtained

$$n^2_{\text{GeSbS}}(\lambda) = 1 + \frac{2.966401\lambda^2}{\lambda^2 - 0.1579334^2} + \frac{0.8449989\lambda^2}{\lambda^2 - 0.3619681^2} + \frac{0.8062024\lambda^2}{\lambda^2 - 26.04563^2}, \quad (2)$$

where the wavelength λ is given in microns. From the index spectrum, the material dispersion parameter is calculated as shown in Fig. 3(b). In comparison, the material dispersion of SiO_2 is also included based on its Sellmeier equation reported in [32]. GeSbS has a large normal dispersion of $D = -250.9$ ps/(nm·km) around 1.55 μm. To achieve broadband phase matching for frequency comb generation, a close-to-zero anomalous dispersion is favorable [19], [28], [29], [30]. This requires geometric dispersion engineering. In a single-wedge-angle disk resonator, as the wavelength increases, the optical mode moves inward (towards the symmetric axis) and the effective mode index decreases, which contributes to normal dispersion [28]. In the reflowed wedge resonator case, we can design the reflow bump to trap the optical mode within the bump, stopping the mode from migrating inward and maintaining tight confinement. This way, we can engineer the effective index n_{eff} by tuning the width and height of the reflow bump similarly to tuning the width and height of a strip waveguide. Experimentally, we can repeatably create reflow bump widths L from 3 to 20 μm with $\pm$ 0.5 μm accuracy by controlling the reflow time at 465 °C [33]. The overall yield of the fabrication process is 40-50% due to the cracks sometimes developing after the BOE etching step. In terms of mode selection, TM modes, with polarization perpendicular to substrate plane, are affected more strongly by the geometry. Thus, we choose TM_{00} mode, as shown in Fig. 4(a), as the target mode for dispersion engineering.

Experimentally, the dispersion of a microresonator is usually expressed as a function of the relative mode number μ centered at the reference resonance frequency, ω_0. The neighboring resonance frequencies can then be written as a Taylor expansion around the reference resonance frequency as

$$\omega_\mu = \omega_0 + D_1\mu + \frac{1}{2}D_2\mu^2 + \frac{1}{6}D_3\mu^3 + \frac{1}{24}D_4\mu^4 + \dots$$
$$= \omega_0 + D_1\mu + D_{int}, \quad (3)$$

where $D_1/2\pi$ is exactly the FSR around the reference resonance, and the sum of all higher order terms is defined as the integral dispersion D_{int} [28]. To simulate the dispersion of reflowed wedge resonators, iterative eigenmode simulations are performed using COMSOL Multiphysics. First, the resonance wavelength of the m^{th} azimuthal mode is guessed to be $\lambda_{\text{guess}} = 2.2 \cdot 2\pi R/m$. Using the refractive index at λ_{guess} given by (2), COMSOL finite element method (FEM) simulation calculates the eigenmode to obtain the new resonance wavelength, λ_{res} , and update the refractive index accordingly. This process is repeated until convergence, which is typically achieved after around 5 iterations. We fix the radius to be 300 μm and the disk thickness 1 μm which are easily achievable by our fabrication process, and then sweep the reflow bump width L and height z_{bump} to find a reflowed geometry that provides near-zero anomalous dispersion around the wavelength of 1575 nm, which is the center wavelength of our tunable NIR laser. As shown in Fig. 4(b) and (c), the resonator with large bump width L or bump height z_{bump} tends to exhibit anomalous dispersion at frequencies lower than the center resonance frequency of 190 THz and normal dispersion at higher frequencies. For fixed radius R and device thickness t, we can engineer the high frequency dispersion into anomalous region as well by decreasing L or z_{bump} or both, which promotes anomalous geometric dispersion due to a tighter mode confinement. Fabrication wise, we can tune the volume of the GeSbS overhang before reflow [Fig. 2(a)] by controlled BOE etch to achieve the desired combination of L and z_{bump}. The overhang volume is also affected by the radius and thickness of the GeSbS disk which are minor factors for dispersion engineering.

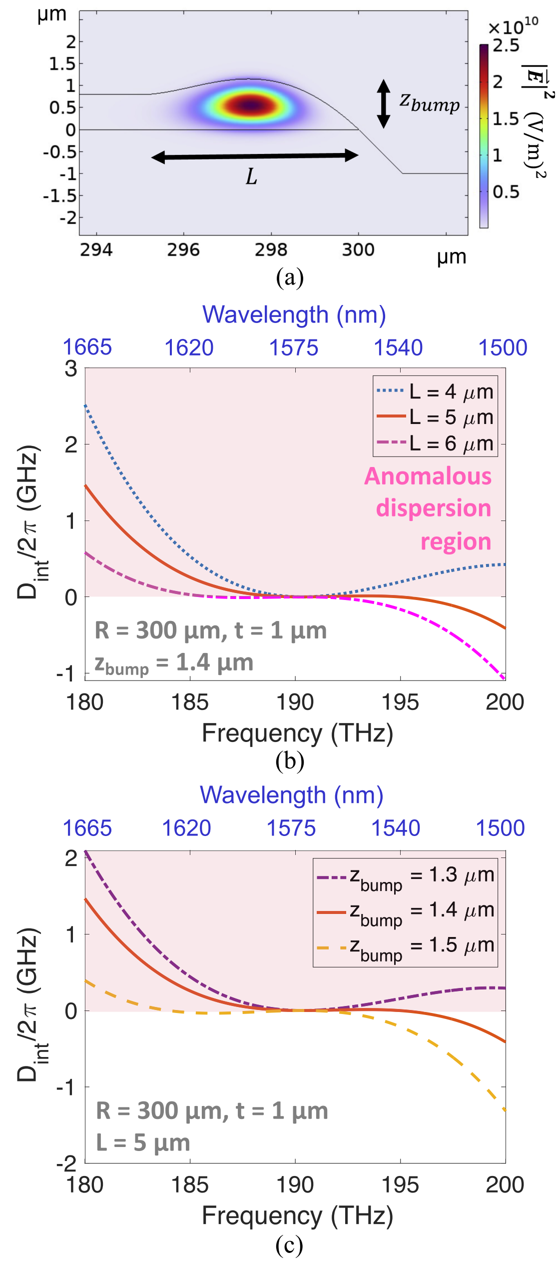

Fig. 4. (a) Illustration of TM_{00} mode profile in a reflowed wedge from finite-element method simulation. The E-field polarization is perpendicular to substrate plane. (b) Simulated TM_{00} mode integrated dispersion D_{int} spectra of various reflowed bump width L, with the same radius of 300 μm, disk thickness of 1 μm and reflow bump height z_{bump} of 1.4 μm. A smaller L leads to a larger anomalous geometric dispersion. (c) Simulated TM_{00} mode integrated dispersion D_{int} spectra of various reflowed bump height z_{bump} show that a smaller z_{bump} also leads to a larger anomalous geometric dispersion.

III. Results and Discussion

High index As_2S_3 tapered fiber is used to couple light into the dispersion engineered TM_{00} mode of our reflowed wedge resonators and characterize their loss and dispersion. An automated fiber tapering setup, composed of a heater and synchronized translation stage, creates As_2S_3 tapered fibers with tapered waists of 0.6 $\sim$ 2 μm (corresponding to effective index of 1.8 $\sim$ 2.4). The transmitted light from a mode-hop-free tunable CW laser (Toptica DLC Pro) through the tapered fiber is captured by an InGaAs detector (Thorlabs DET10C). To calibrate the laser scan over 90 nm wavelength range, a portion of the laser output was also monitored after transmission through a fiber Mach–Zehnder interferometer (MZI) with a 20.8 MHz FSR.

Based on the simulation results, we choose resonators with a bump width $L = 6$ μm and height $z_{\text{bump}} = 1.4$ μm and characterized their dispersion. The radius of the resonators is set to be $200 - 400\ \mu$m to have abundant resonances within our laser scanning range. To selectively couple with the TE polarization modes, we move the resonator along the tapered fiber from the thicker part towards the thinner part, while continuously rotating the fiber polarization controller to change the input polarization between TE and TM. The TE_{00} mode with the largest effective index can be identified as the first set of observed resonance dips. It also has the largest FSR among all TE and TM modes. By fine-tuning the fiber polarization controller, we can optimize the coupling with the TE_{00} mode. For coupling with TM modes, we adjust the fiber polarization controller until all TE coupling is eliminated. We then begin to observe transmission dips due to TM modes. For both polarizations, moving the resonator further towards the thinner part of the tapered fiber will reveal additional higher order modes which can distinguished from the fundamental modes by the smaller FSRs. By fine-tuning the coupling condition between the tapered fiber and the resonators, broadband coupling with the TM_{00} and TE_{00} mode can be achieved as shown in their broadband transmission spectra Fig. 5(a) and (b). The TE_{00} mode has the largest FSR of 89.1 GHz among the resonator's WGMs and an intrinsic Q factor of 1.5×10^5. The TM_{00} mode has a slightly smaller FSR of 87.8 GHz and a higher intrinsic Q factor of 1.9×10^5. The resonance frequencies are then determined by fitting each transmission peak from the spectra to calculate the integral dispersion D_{int} using (3) around center wavelength of 1575 nm, as shown in Fig. 5(c). The dispersion engineered TM_{00} mode clearly shows a flattened anomalous dispersion compared to the TE_{00} mode that has large normal dispersion similar to the material dispersion. This result showcases our capabilities of dispersion engineering in the reflowed wedge resonator platform that is very promising for four-wave-mixing and micro comb generation.

For nonlinear photonic devices, high quality factor and low propagation loss are as crucial as dispersion engineering. The optical transmission of a few reflowed wedge resonators with different geometries are analyzed for loss characterization. For each resonance, the transmission dip is fitted with a Lorentzian line-shape to obtain the loaded quality factor $Q_{\text{load}} = \frac{\lambda_{\text{res}}}{\Delta\lambda_{\text{FWHM}}}$, where λ_{res} is the resonance wavelength and $\Delta\lambda_{\text{FWHM}}$ is the full width at half maximum of the resonance. The intrinsic quality factor Q is calculated as $Q = \frac{2Q_{\text{load}}}{1+T}$, where T is the coupling depth normalized to 1. As shown in Fig. 6(a), the highest Q from the GeSbS reflowed wedge resonators is 1.2×10^6 for the TE_{10} mode of a 80 μm-radius, 3.6 μm-thick reflowed wedge resonator coated with poly(methyl methacrylate) cladding. The polymer coating can protect the smooth reflowed surface from dust and other chemical contamination, leading to high Q. However, the dip-coating process used in this work is not very reliable and may produce substantial variations in thickness, which in turn could complicate dispersion engineering. Without polymer coating, a 5.5 μm-thick reflowed wedge has a quality factor of 5.3×10^5 for its TM_{00} mode [Fig. 6(b)], but the reflow bump is still too thick to effectively confine the mode migration for dispersion control. On the thinner dispersion engineered reflowed wedge with 1 μm disk thickness, the TM_{00} mode with anomalous dispersion around 1550 nm has a quality factor of 1.9×10^5

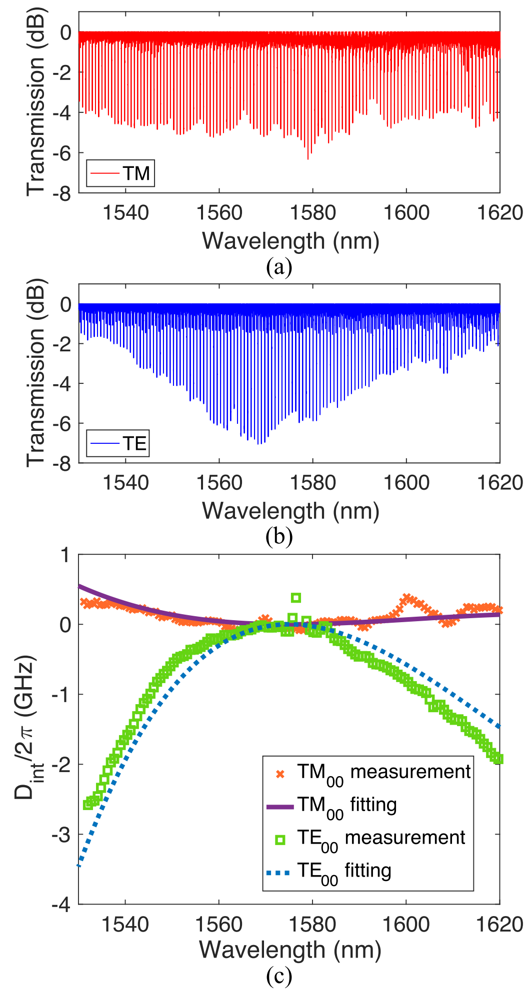

Fig. 5. (a) The TM polarization and (b) TE polarization transmission spectrum of a 250 μm-radius reflowed wedge resonator over 90 nm wavelength bandwidth. (c) The measured integral dispersion D_{int} of both the TE_{00} and TM_{00} modes of the 250 μm-radius reflowed wedge resonator. The dispersion engineered TM_{00} mode clearly shows a flatter anomalous dispersion compared to the TE_{00} mode's large normal dispersion.

TABLE I
CALCULATED PROPAGATION LOSSES OF VARIOUS REFLOWED WEDGE RESONATORS

Thickness	Mode	Clad	Intrinsic Q	Loss α
1.0 μm	TM_{00}	Air	1.9×10^5	2.16 dB/cm
5.5 μm	TM_{00}	Air	5.3×10^5	0.76 dB/cm
3.6 μm	TE_{10}	PMMA	1.2×10^6	0.34 dB/cm

[Fig. 6(c)]. The propagation loss can be calculated by

$$\alpha = \frac{2\pi n_{\text{eff}}}{\lambda Q}, \quad (4)$$

where n_{eff} is calculated from the FSR. A summary of the calculated losses from reflowed wedge resonators is shown in Table I.

Using scanning electron microscopy (SEM), the line-edge roughness of reflowed wedge resonators is found to be $\sigma_{\text{rms}} =$ 5.0 nm, and the lateral correlation length $L_c = 250$ nm, which

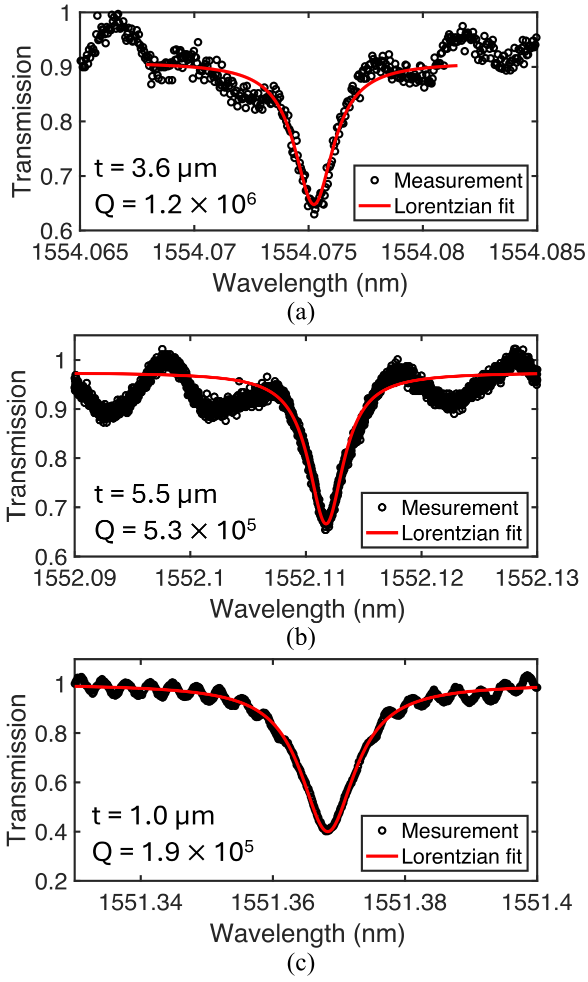

Fig. 6. Resonance transmission dip and its Lorentzian fit for (a) the TE_{10} mode of a 80 μm-radius, 3.6 μm-thick reflowed wedge resonator coated with poly(methyl methacrylate)) (PMMA) cladding, (b) the TM_{00} mode of a 100 μm-radius, 5.5 μm-thick, air-clad reflowed wedge resonator, (c) the TM_{00} mode of the dispersion engineered, 250 μm-radius, 1.0 μm-thick, air-clad reflowed wedge resonator, whose dispersion is characterized in Fig. 5.

are close to the resolution limit of the UV lithography [34]. For the 1.0 μm-thick reflowed wedge resonator, the optical mode is tightly confined and can be approximately treated as a waveguide for which one can use the Payne-Lacey model [35] to estimate the scattering loss. In our devices, despite the ultrasmooth top and bottom surfaces of the reflow bump, the loss caused by a sidewall with 5 nm line-edge roughness is estimated to be 1.5 dB/cm for the TM_{00} mode. For the 5.5 μm-thick reflowed wedge, the waveguide approximation of the Payne-Lacey model is no longer applicable. Qualitatively, however, we can expect the decreased mode overlap with the resonator surface should reduce the loss, which agrees with the experimental observation.

While the reduced mode overlap with the resonator surface is favorable for high Q factors, it diminishes the ability to engineer dispersion. Therefore, an optimal trade-off must be found between minimizing loss and maintaining strong dispersion engineering capabilities to fully leverage the potential of chalcogenide wedge resonators for nonlinear optical applications. Still, the achieved quality factors in our chalcogenide resonators remain magnitudes lower than those reported for ultra-high-Q reflowed silica microresonators, which can exceed 10^8 due to the exceptionally low material absorption and near-atomically smooth surface [23]. While reflow-assisted fabrication significantly enhances the surface smoothness of our chalcogenide resonators, their intrinsic material absorption still presents a fundamental limitation compared to silica. Previous studies on chalcogenide microresonators have reported the best Q factors in the range of 10^6 – 10^7 [36], [37], [38], indicating that further reduction in our devices' loss will require addressing both scattering and material absorption constraints.

IV. Conclusion

In conclusion, we present a thermal-reflow-assisted fabrication method that creates $Ge_{23}Sb_7S_{70}$ reflowed wedge resonators with excellent surface roughness and quality factors exceeding 10^6. Our simulations of thin reflowed wedges show the ability to engineer the dispersion of WGMs to overcome large material dispersion in near-infrared wavelength and achieve anomalous dispersion. We have successfully fabricated the reflow bump geometry prescribed by the simulations and experimentally demonstrated an engineered flat anomalous dispersion of the TM_{00} mode. These results showcase that reflowed wedge geometry offers a greater degree of freedom for dispersion engineering than most WGM microresonators while maintaining high quality factor, promising a new path to high quality chalcogenide resonators nonlinear optical applications.

Acknowledgment

The authors gratefully acknowledge Dr. Kyuyoung Bae for developing the fabrication process of GeSbS reflowed wedge resonators. The authors would also like to thank Thariq Shanavas, Greg Krueper and James Erikson for useful technical discussions.

References

[1] S. Tanabe, "Rare-earth-doped glasses for fiber amplifiers in broadband telecommunication," *Comptes Rendus Chim.*, vol. 5, no. 12, pp. 815–824, Dec. 2002, doi: 10.1016/S1631-0748(02)01449-2.

[2] N. Hoghooghi et al., "Broadband 1-GHz mid-infrared frequency comb," *Light Sci. Appl.*, vol. 11, no. 1, Sep. 2022, Art. no. 264, doi: 10.1038/s41377-022-00947-w.

[3] Y. Jin et al., "Long wavelength mid-infrared multi-gases spectroscopy using tunable single-mode slot waveguide quantum cascade laser," *Opt. Exp.*, vol. 31, no. 17, pp. 27543–27552, Aug. 2023, doi: 10.1364/OE.495160.

[4] H. Mahmudlu et al., "Fully on-chip photonic turnkey quantum source for entangled qubit/qudit state generation," *Nature Photon.*, vol. 17, no. 6, pp. 518–524, Jun. 2023, doi: 10.1038/s41566-023-01193-1.

[5] J. G. Fujimoto, C. Pitris, S. A. Boppart, and M. E. Brezinski, "Optical coherence tomography: An emerging technology for biomedical imaging and Optical biopsy," *Neoplasia N. Y. N*, vol. 2, no. 1–2, pp. 9–25, Jan. 2000.

[6] F. Smektala, C. Quemard, V. Couderc, and A. Barthélémy, "Non-linear optical properties of chalcogenide glasses measured by Z-scan," *J. Non-Cryst. Solids*, vol. 274, no. 1, pp. 232–237, Sep. 2000, doi: 10.1016/S0022-3093(00)00215-5.

[7] J. W. Choi et al., "Nonlinear characterization of GeSbS chalcogenide glass waveguides," *Sci. Reports*, vol. 6, no. 1, Dec. 2016, Art. no. 39234, doi: 10.1038/srep39234.

[8] K. S. Bindra, H. T. Bookey, A. K. Kar, B. S. Wherrett, X. Liu, and A. Jha, "Nonlinear optical properties of chalcogenide glasses: Observation of multiphoton absorption," *Appl. Phys. Lett.*, vol. 79, no. 13, pp. 1939–1941, Sep. 2001, doi: 10.1063/1.1402158.

[9] M. Grayson, M. Zohrabi, K. Bae, J. Zhu, J. T. Gopinath, and W. Park, "Enhancement of third-order nonlinearity of thermally evaporated GeSbSe waveguides through annealing," *Opt. Exp.*, vol. 27, no. 23, pp. 33606–33620, Nov. 2019, doi: 10.1364/OE.27.033606.

[10] M. Grayson et al., "Fabrication and characterization of high quality GeSbSe reflowed and etched ring resonators," *Opt. Exp.*, vol. 30, no. 17, pp. 31107–31121, Aug. 2022, doi: 10.1364/OE.468249.

[11] M. Grayson et al., "On-chip mid-infrared optical sensing with GeSbSe waveguides and resonators," *Opt. Exp.*, vol. 31, no. 2, pp. 877–889, Jan. 2023, doi: 10.1364/OE.476186.

[12] Z. Yang et al., "Efficient acousto-optic modulation using a microring resonator on a thin-film lithium niobate–chalcogenide hybrid platform," *Opt. Lett.*, vol. 47, no. 15, pp. 3808–3811, Aug. 2022, doi: 10.1364/OL.464482.

[13] L. Wan et al., "Highly efficient acousto-optic modulation using nonsuspended thin-film lithium niobate-chalcogenide hybrid waveguides," *Light Sci. Appl.*, vol. 11, no. 1, May 2022, Art. no. 145, doi: 10.1038/s41377-022-00840-6.

[14] Z. Han et al., "On-chip chalcogenide glass waveguide-integrated mid-infrared PbTe detectors," *Appl. Phys. Lett.*, vol. 109, no. 7, Aug. 2016, Art. no. 071111, doi: 10.1063/1.4961532.

[15] V. B. Braginsky, M. L. Gorodetsky, and V. S. Ilchenko, "Quality-factor and nonlinear properties of optical whispering-gallery modes," *Phys. Lett. A*, vol. 137, no. 7, pp. 393–397, May 1989, doi: 10.1016/0375-9601(89)90912-2.

[16] J. Ward and O. Benson, "WGM microresonators: Sensing, lasing and fundamental optics with microspheres," *Laser Photon. Rev*, vol. 5, no. 4, pp. 553–570, 2011, doi: 10.1002/lpor.201000025.

[17] H. Lee et al., "Chemically etched ultrahigh-Q wedge-resonator on a silicon chip," *Nature Photon.*, vol. 6, no. 6, pp. 369–373, Jun. 2012, doi: 10.1038/nphoton.2012.109.

[18] F. Ramiro-Manzano, N. Prtljaga, L. Pavesi, G. Pucker, and M. Ghulinyan, "A fully integrated high-Q whispering-gallery wedge resonator," *Opt. Exp.*, vol. 20, no. 20, pp. 22934–22942, Sep. 2012, doi: 10.1364/OE.20.022934.

[19] K. Y. Yang et al., "Broadband dispersion-engineered microresonator on a chip," *Nature Photon.*, vol. 10, no. 5, pp. 316–320, May 2016, doi: 10.1038/nphoton.2016.36.

[20] B. Xu, M. Grayson, T. Shanavas, J. T. Gopinath, and W. Park, "Dispersion control of high-quality $Ge_{23}Sb_7S_{70}$ reflowed wedge resonators," in *presented at CLEO 2023*, San Jose, CA, USA, May 07–12, 2023, Paper JW2A.13, doi: 10.1364/CLEO_AT.2023.JW2A.13.

[21] K. Bae et al., "On-chip high-quality $Ge_{23}Sb_7S_{70}$ round-wedge resonators for broadband dispersion engineering," *presented at Conf. Lasers Electro-Opt.*, Washington, DC, USA, May 10–15, 2020, PaperAF1K.2, doi: 10.1364/CLEO_AT.2020.AF1K.2.

[22] J. Song et al., "Stimulated brillouin scattering in low-loss $Ge_{25}Sb_{10}S_{65}$ chalcogenide waveguides," *J. Lightw. Technol.*, vol. 39, no. 15, pp. 5048–5053, Aug. 2021, doi: 10.1109/JLT.2021.3078722.

[23] D. K. Armani, T. J. Kippenberg, S. M. Spillane, and K. J. Vahala, "Ultra-high-Q toroid microcavity on a chip," *Nature*, vol. 421, no. 6926, pp. 925–928, Feb. 2003, doi: 10.1038/nature01371.

[24] P. Del'Haye, S. A. Diddams, and S. B. Papp, "Laser-machined ultra-high-Q microrod resonators for nonlinear optics," *Appl. Phys. Lett.*, vol. 102, no. 22, Jun. 2013, Art. no. 221119, doi: 10.1063/1.4809781.

[25] A. Dutt, K. Luke, S. Manipatruni, A. L. Gaeta, P. Nussenzveig, and M. Lipson, "On-chip optical squeezing," *Phys. Rev. Appl.*, vol. 3, no. 4, Apr. 2015, Art. no. 044005, doi: 10.1103/PhysRevApplied.3.044005.

[26] T. J. Kippenberg, S. M. Spillane, and K. J. Vahala, "Kerr-nonlinearity optical parametric oscillation in an ultrahigh-*Q* toroid microcavity," *Phys. Rev. Lett.*, vol. 93, no. 8, Aug. 2004, Art. no. 083904, doi: 10.1103/PhysRevLett.93.083904.

[27] K. Luke, Y. Okawachi, M. R. E. Lamont, A. L. Gaeta, and M. Lipson, "Broadband mid-infrared frequency comb generation in a Si_3N_4 microresonator," *Opt. Lett.*, vol. 40, no. 21, pp. 4823–4826, Nov. 2015, doi: 10.1364/OL.40.004823.

[28] S. Fujii and T. Tanabe, "Dispersion engineering and measurement of whispering gallery mode microresonator for Kerr frequency comb generation," *Nanophotonics*, vol. 9, no. 5, pp. 1087–1104, May 2020, doi: 10.1515/nanoph-2019-0497.

[29] P. Grelu and N. Akhmediev, "Dissipative solitons for mode-locked lasers," *Nature Photon.*, vol. 6, no. 2, pp. 84–92, Feb. 2012, doi: 10.1038/nphoton.2011.345.

[30] T. Herr et al., "Temporal solitons in optical microresonators," *Nature Photon.*, vol. 8, no. 2, pp. 145–152, Feb. 2014, doi: 10.1038/nphoton.2013.343.

[31] W. Sellmeier, "Ueber die durch die Aetherschwingungen erregten Mitschwingungen der Körpertheilchen und deren Rückwirkung auf die ersteren, besonders zur Erklärung der Dispersion und ihrer Anomalien," *Ann. Phys.*, vol. 223, no. 11, pp. 386–403, 1872, doi: 10.1002/andp.18722231105.

[32] I. H. Malitson, "Interspecimen comparison of the refractive index of fused silica∗,†," *J. Opt. Soc. America*, vol. 55, no. 10, pp. 1205–1209, Oct. 1965, doi: 10.1364/JOSA.55.001205.

[33] B. Xu, "Chalcogenide microresonators for near- and mid-infrared nonlinear photonics," Ph.D. dissertation, Univ. Colorado Boulder, Boulder, CO, USA, 2024, [Online]. Available: https://www.proquest.com/openview/6c47d6c7c9ab2454510b523d01f74b2e/1?pq-origsite=gscholar&cbl=18750&diss=y

[34] D. B. Miller, "Resolution enhancement in photolithography via STED inspired process and novel mask development," Ph.D. dissertation, Univ. Colorado Boulder, Boulder, CO, USA, 2020. [Online]. Available: https://www.proquest.com/docview/2447027558/abstract/1447086900164863PQ/1?sourcetype=Dissertations%20&%20Theses

[35] F. P. Payne and J. P. R. Lacey, "A theoretical analysis of scattering loss from planar optical waveguides," *Opt. Quantum Electron.*, vol. 26, no. 10, pp. 977–986, Oct. 1994, doi: 10.1007/BF00708339.

[36] J. Zhu, T. M. Horning, M. Zohrabi, W. Park, and J. T. Gopinath, "Photo-induced writing and erasing of gratings in As_2S_3 chalcogenide microresonators," *Optica*, vol. 7, no. 11, pp. 1645–1648, Nov. 2020, doi: 10.1364/OPTICA.405136.

[37] B. Zhang et al., "On-chip chalcogenide microresonators with low-threshold parametric oscillation," *Photon. Res.*, vol. 9, no. 7, pp. 1272–1279, Jul. 2021, doi: 10.1364/PRJ.422435.

[38] K. Ko et al., "A mid-infrared Brillouin laser using ultra-high-Q on-chip resonators," *Nat. Commun.*, vol. 16, no. 1, Mar. 2025, Art. no. 2707, doi: 10.1038/s41467-025-58010-2.